

# Advanced Gesture Recognition in Autism: Integrating YOLOv7, Video Augmentation and VideoMAE for Video Analysis

Amit Kumar Singh<sup>[0009-0000-3900-4015]</sup>, Trapti Shrivastava<sup>[0000-0001-8455-282X]</sup>, and Vrijendra Singh<sup>[0000-0002-8818-5673]</sup>

Department of Information Technology,  
Indian Institute of Information Technology, Allahabad, 211013, India {amitramraj005,shri.taps02}@gmail.com  
vrij@iiita.ac.in

**Abstract.** Deep learning and advancements in contactless sensors have significantly enhanced our ability to understand complex human activities in healthcare settings. In particular, deep learning models utilizing computer vision have been developed to enable detailed analysis of human gesture recognition, especially repetitive gestures which are commonly observed behaviors in children with autism. This research work aims to identify repetitive behaviors indicative of autism by analyzing videos captured in natural settings as children engage in daily activities. The focus is on accurately categorizing real-time repetitive gestures such as spinning, head banging, and arm flapping. To this end, we utilize the publicly accessible Self-Stimulatory Behavior Dataset (SSBD) to classify these stereotypical movements. A key component of the proposed methodology is the use of **VideoMAE**, a model designed to improve both spatial and temporal analysis of video data through a masking and reconstruction mechanism. This model significantly outperformed traditional methods, achieving an accuracy of 97.7%, a 14.7% improvement over the previous state-of-the-art. This demonstrates the efficacy of VideoMAE in extracting and learning robust features for the classification of complex repetitive gestures.

Additionally, the research incorporates **YOLOv7** (You Only Look Once, version 7), a real-time object detection model that enhances the precision of detecting and segmenting objects within video frames. YOLOv7, known for its speed and efficiency. In this study, YOLOv7 helps preprocess the videos by identifying and masking the largest object of interest in each frame, which is crucial for focusing on repetitive gestures without distractions from irrelevant details. Another crucial aspect of the research is the use of **video augmentation** techniques to diversify and enrich the dataset, especially given the limited and noisy nature of SSBD videos.

**Keywords:** Autism · Stereotypical Repetitive Behaviours · VideoMAE · SSBD Video Data · Masked Autoencoding · Self-supervised Learning · Video Analysis

## 1 INTRODUCTION

Repetitive behavioral patterns and difficulty with communication and social interaction are among the many symptoms together referred to as autism spectrum disorder (ASD) [30]. According to the CDC's Autistic and Developmental Disabilities Monitoring (ADDM) Network, about 1 in 44 American children received an ASD diagnosis in 2020 [10]. In 2018, Dr. Narendra Arora [6] carried out a research across many Indian areas and discovered that one in every eight children has at least one neurodevelopmental problem and one in every 100 people under the age of ten has autism. Opinions from pediatricians and parents are essential for the early diagnosis of ASD. New study, however, indicates that many children do not receive a conclusive diagnosis for autism until they are much older (beyond the age of three) [20]. It's still challenging to identify and diagnose ASD in children before the age of two.

Numerous behavioral and motor characteristics, including stereotypically repetitive motions, can be used to diagnose autism. Such repeated motions are usually the result of passion, anxiety, or fury. Among the signs of autism are erratic behaviors that occur unexpectedly and for short bursts of time. Most of the time, the youngster hurts himself with these motions. Sadly, parents could fail to see these motions and fail to notice them. It is essential to identify these repeated actions in order to diagnose autism in youngsters. Psychologists must spend time and money monitoring their behavior, and the financial burden falls on the

family. Recent advancements in technology and deep learning algorithms have made it feasible for artificial intelligence devices to automatically recognize self-stimulatory movements.

The aim of this study is to develop a model capable of recognizing children’s repetitious behavior. This would assist doctors in selecting the most appropriate behavioral therapy and provide family support in remote places where access to state-of-the-art diagnostic technologies is limited.

With the use of contemporary technologies like computer vision and deep learning models, it may be possible to identify children’s stereotypical repetitive motions in order to provide a precise diagnosis and prompt therapy intervention. This work developed a real-time computer vision and deep learning system to monitor and identify archetypal repetitive behavior in youngsters.

- We designed a novel model by leveraging the VideoMAE model for video classification, which combines masked autoencoders for feature extraction and attention mechanisms for gesture classification, and trained this model for the detection of stereotypical repetitive autistic behaviors.
- Our trained VideoMAE model performs significantly better than prior vision-based techniques, according to experimental results on the Self-Stimulatory Behavior Dataset (SSBD) [26]. This provides a solid baseline for the detection of stereotypical repetitive autistic actions in videos.

## 2 RELATED WORK

Various approaches have been developed by researchers to examine and monitor behavior to identify autism, such as questionnaires [2, 7, 17, 23, 24], eye gaze [8, 9, 15, 16], functional magnetic resonance imaging (fMRI) [4, 11, 14, 19, 35], facial feature analysis [1, 5, 28] and multiple modalities in a single study [21, 22, 32]. Most of these studies aim to identify and classify ASD and typical-developed children with different modalities of data. In addition, stereotypical repetitive autistic behaviors have been used to evaluate autism, with most researchers using the SSBD dataset [26]. To evaluate autism with autistic behavior firstly, it is important to classify these stereotypical repetitive behaviors.

In the early years, the researcher used haar cascade for person detection and classified the gestures using basic ML or DL algorithms such as MLP, SVM, DCNN, ConvLSTM, etc., and achieved an accuracy of 79% [25]. The SSBD was proposed by Rajagopalan et al. [26, 27] and comprises movies showing autistic children going about their regular lives. They combined a histogram of optical flow with a histogram of dominating movements. Their three-way challenge headbanging, spinning, and hand-flapping classification model produced an accuracy of 76.3%. Single CNN was used to extract the features from each input sequence of headbanging videos and fed into LSTM for further classification. Deng A et al. [12] introduced the video swin transformer for analyzing autistic behaviors and combined visual features with language information and achieved an accuracy of 97%. Washington et al. [33] presented a new model and achieved the mean F1-score of 90.77%. Anish et al. [18] implemented LSTM and MobileNetV2 on SSBD for abnormal hand movement classification, achieving an F1 score of  $75.2 \pm 0.6$ . Wei et al. [34] Employed MS-TCN on a modified SSBD dataset, achieving 84% weighted F1 score. They addressed the noise problem in the dataset and resolved it by replacing 11 videos from the actual dataset. Dia et al. [13] Utilized the Perceive model on SSBD and Affect-Net datasets, focusing on facial expressions in ASD children, with 74.5% accuracy. An approach for the behavioral diagnosis of ASD was created by Ali et al. [3]. During the time of their ASD diagnosis, they gathered and documented a collection of recordings of stereotypical children’s behavior captured in an uncontrolled setting. The dataset contained 388 videos of 5 categories and combined of the two streams of Inflated 3D Networks (I3D) produced the greatest accuracy (85.6 to 86.04%).

However, these state-of-the-art works recognize stereotypical repetitive autistic behaviors in autistic children on the SSBD dataset are not very optimized (less than 78%). We also find that the publicly available dataset has a very small amount of data with a high amount of noise due to being collected from an uncontrolled environment. The initial research work did not acquire features very accurately due to noisy data.

To address these issues, we have implemented the VideoMAE model, which combines masked autoencoders for improved feature extraction and attention mechanisms to optimize the classification performance.

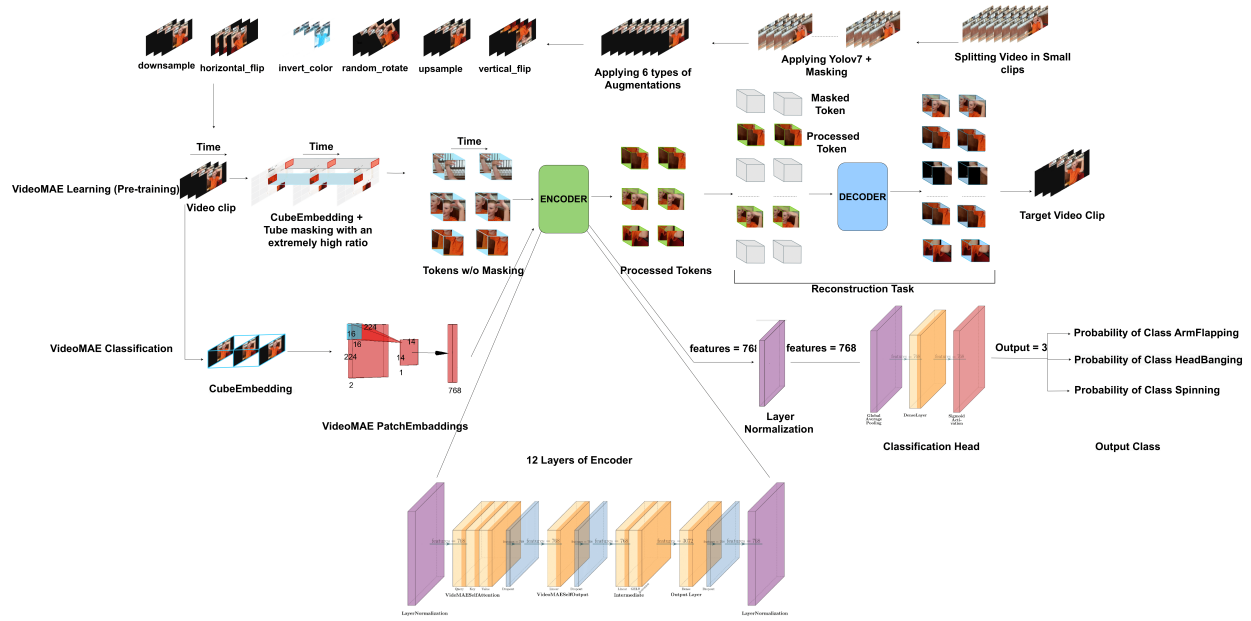


Fig. 1. Work Flow of VideoMAE based model

### 3 MATERIAL AND METHODS

Among children with ASD, stereotypical repeated movements are one of the most often seen stimming activities. Three different types of repeated gestures are taken into consideration in this study: arm flipping, head banging, and spinning. These behaviors are characterized by recurrent actions that may only continue for a moment. There are several ways in which arm flapping might appear as a stimming behavior: jerking fingers, clicking fingers, and massive arm movements.

Children with autism are susceptible to headbanging, a kind of stimming activity in which they repeatedly strike their head against something like a floor, furniture, door, etc. This might lead to self-harm. Another stimming habit is spinning, in which a child spins things or themselves. Children with autism often utilize these behaviors to control sensory input or to deal with stress or excitement. Obtaining a video dataset is the first stage in our work. The second stage involves trimming the SSBD videos, where the videos are segmented into smaller, more manageable clips. In the third stage, YOLOv7 with masking is applied to these trimmed videos, allowing for precise object detection and masking within each segment. The fourth stage focuses on applying video augmentations, which involves employing various augmentation techniques to increase the diversity and robustness of the video data. These stages collectively prepare the data for further analysis and model training, ultimately supporting the project's goals of effective behavior analysis. (as illustrated in Fig 1).

### 3.1 SSBD DATASET

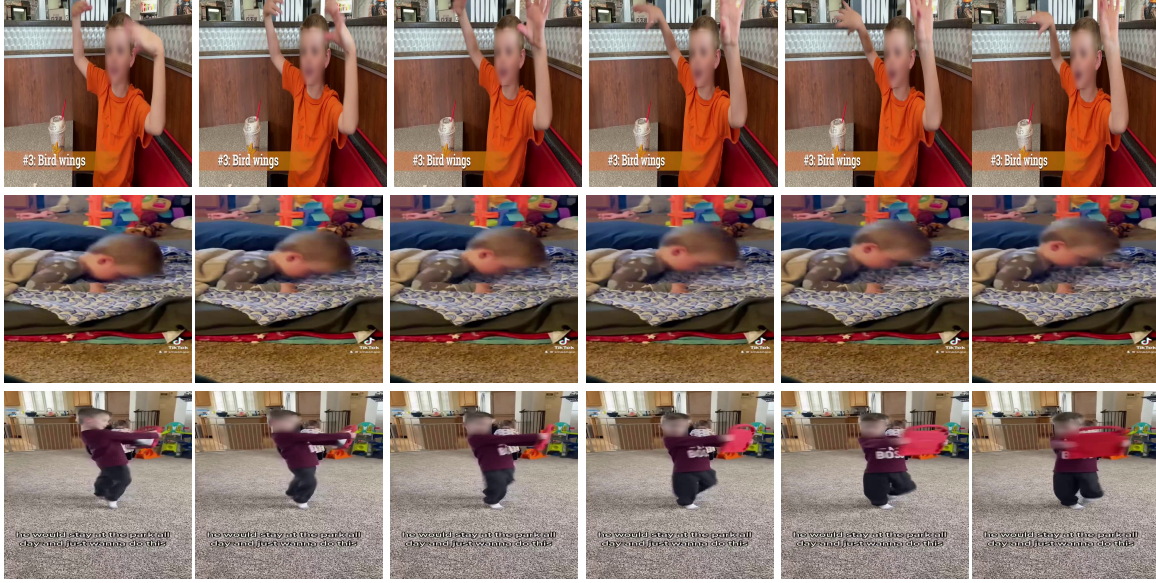


**Fig. 2.** Each class includes a frame depicting a certain action. The first row illustrates arm flapping, the second row illustrates head pounding, and the last row illustrates spinning motion [26]

The study utilizes Self-Stimulatory Behavioural Data (SSBD) [26], which is specifically designed to aid in the identification and analysis of stereotypical repetitive behaviors in autistic children. It’s a comprehensive dataset comprising video recordings of children exhibiting self-stimulatory stimming behaviors of three different kinds: arm flapping, head banging, and spinning (Fig 2). These ”stimming” behaviors are characterized by repetitive or unusual movements or noises, often observed in individuals with Autism Spectrum Disorders (ASD). Parents or caregivers captured these videos in unmanaged natural environments.

The SSBD dataset contains a total of 75 videos. Each category includes 25 videos. However, some of the videos are not available at the given URL, due to YouTube privacy concerns. We were able to retrieve only 59 videos: 19 for Spinning, 20 for Head Banging, and 19 for Arm Flapping.

### 3.2 DATA PRE-PROCESSING

**Table 1.** Number of videos in each class before and after pre-processing

Class	SSBD [36]		
	original	trim	augumented
ArmFlapping	25	29	203
HeadBanging	25	41	287
Spinning	25	54	378

The table 1 summarizes the number of videos in each class—ArmFlapping, HeadBanging, and Spinning—before and after pre-processing in the SSBD dataset. Initially, each class contains 25 videos in the original dataset. After trimming, the number of videos increases to 29 for ArmFlapping, 41 for HeadBanging, and 54 for Spinning, indicating the removal of redundant or non-informative segments. With augmentation, the dataset size significantly expands to 203, 287, and 378 videos for ArmFlapping, HeadBanging, and

Spinning, respectively. This augmentation process enhances the dataset’s diversity, aiding in improving model robustness and performance.

**Table 2.** Detailed statistics description for the SSBD dataset, including minimum and maximum frame counts, frame resolutions, sizes, and average video duration across different behaviors like Arm Flapping, Head Banging, and Spinning, both for the original and trimmed datasets

	SSBD			trim_SSBD			trim_SSBD_Aug		
	ArmFlapping	HeadBanging	Spinning	ArmFlapping	HeadBanging	Spinning	ArmFlapping	HeadBanging	Spinning
Min Frame Count	44	31	90	44	14	55	22	7	28
Max Frame Count	713	720	1656	258	227	270	258	227	270
Avg Frame Count	191.04	330.68	407.36	135.65	121.29	147.03	125.99	112.65	136.56
Min Frame Size	204X360	176X144	204X360	204X360	176X144	270X360	204X360	176X144	270X360
Max Frame Size	1280X720	1280X720	1280X720	1280X720	1280X720	1280X720	1920X1080	1920X1080	1920X1080
Avg Frame Size	644.88X486.72	513.04X436.48	580.16X565.76	644.20X477.51	540.24X460.29	702.40X602.81	690.21X511.62	578.82X493.17	752.57X645.87
Avg video duration	7.08 sec	11.79 sec	17.22 sec	5.04 sec	4.41 sec	6.16 sec	4.68 sec	4.10 sec	5.72 sec
Number of videos	25	25	25	29	41	50	203	287	378



**Fig. 3.** Frame from each class, with the first figure showing the arm flapping, the second figure showing the head banging and the last figure showing the spinning behavior after applying Yolov7 and masking. [26]

Videos of the SSBD dataset showcase a variety of behavioral movements from various periods. As a result, it was necessary to trim the parts according to behavioral motions. However, due to YouTube privacy issues, only 58 videos are currently available. To maintain the characteristics of the dataset we added 16 new videos of the same duration and same behavior class as missing videos.

All the Videos were captured in an uncontrolled environment, so there are different types of issues identified in the dataset. For example, too many people in a single frame or only a particular part of the video contain repetitive activity. The dataset was divided into 15% for testing, 15% for validation and 70% for training.

As we can see from the table 2 in the original SSBD dataset, few video are way lengthy then the other video, and these lengthy video have stimming behaviour for very small duration. Since the dataset was already challenging because of being recorded in natural environment and poor light conditions, we decided to break the long video into smaller parts to ease the training and testing process. Total duration of video in all 3 class remains the same before and after trimming. We are calling this trimmed data as trim\_SSBD.

After trimming the longer videos in smaller videos the number of videos in each class is shown in the table 2.

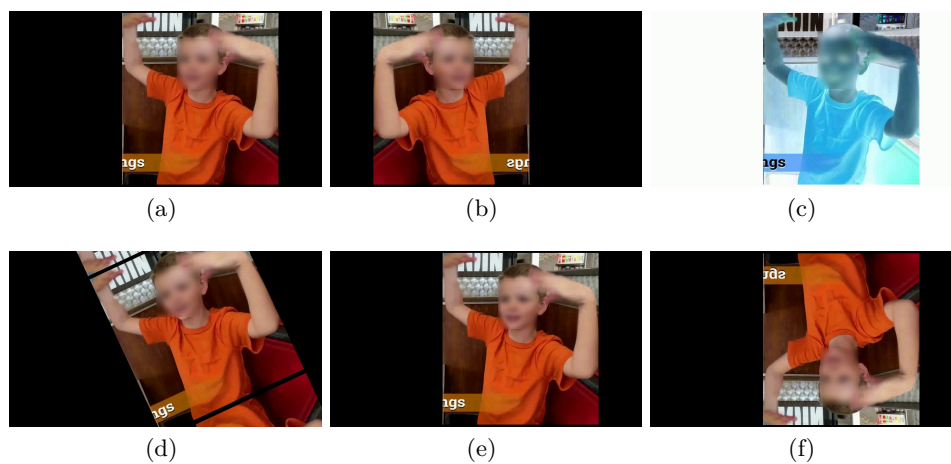


**Fig. 4.** Frames showing the augmentations used after applying Yolov7 and masking. (a) downsample, (b) horizontal flip, (c) Invert color, (d) random rotate, (e) upsample, (f) vertical flip

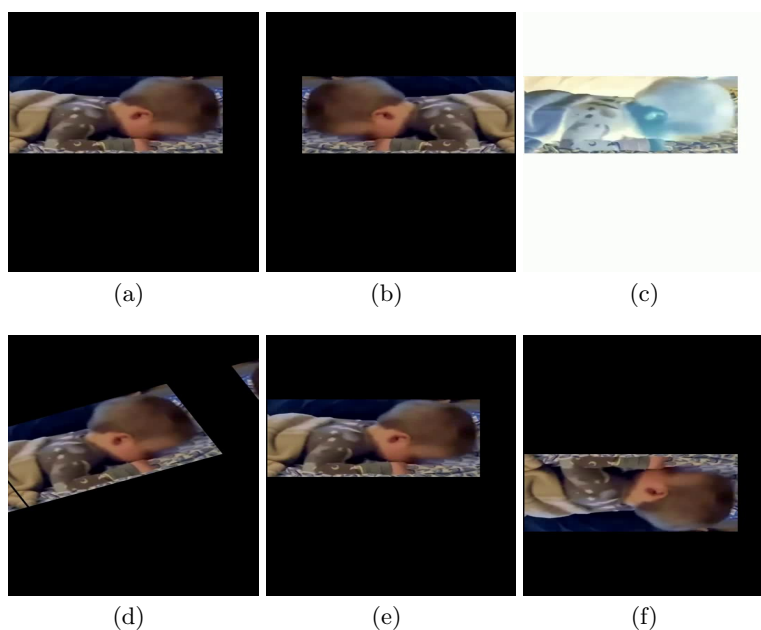


**Fig. 5.** Frames showing the augmentations used after applying Yolov7 and masking. (a) downsample, (b) horizontal flip, (c) Invert color, (d) random rotate, (e) upsample, (f) vertical flip



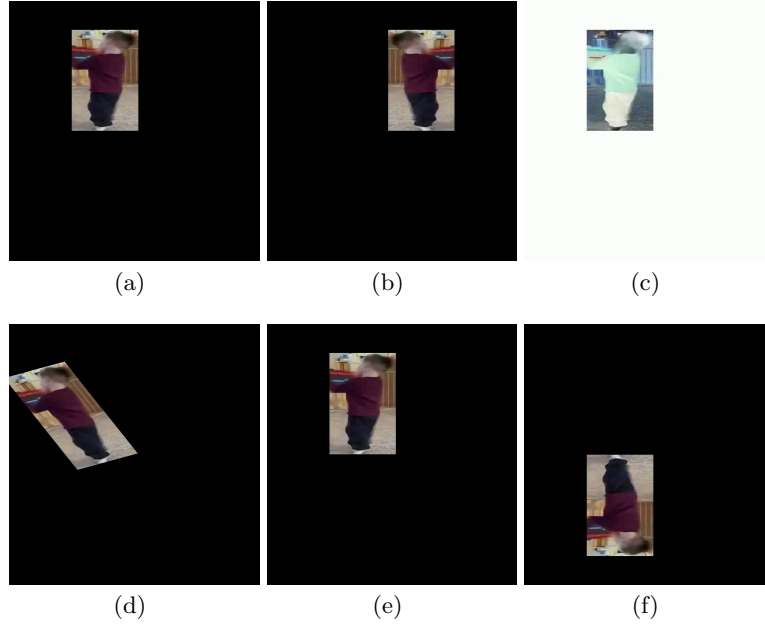


**Fig. 6.** Frames showing the augmentations used after applying Yolov7 and masking. (a) downsample, (b) horizontal flip, (c) Invert color, (d) random rotate, (e) upsample, (f) vertical flip

After trimming the videos into smaller one, we can see in table 2 that after trimming the videos the overall video duration dropped from 12 sec/video to 5.32 sec/video.

From each video, we took out all frames, which we then preprocessed as follows. All the videos are collected from different resources, so each video has a different dimension. The average height and width of videos is 635 x 526. Since the VideoMAE model requires an input size of 224 x 224, we resized the frames accordingly to fit this requirement.

The table also details the frame sizes for each dataset. The SSBD dataset has a range of frame sizes, with the minimum sizes being 204x360 for Arm Flapping, 176x144 for Head Banging, and 204x360 for Spinning. The maximum frame size for all behaviors in the SSBD dataset is 1280x720. The average frame sizes are 644.88x486.72 for Arm Flapping, 513.04x436.48 for Head Banging, and 580.16x565.76 for Spinning.

For the Modified SSBD dataset, the minimum frame sizes are consistent with the SSBD dataset at 204x360 for Arm Flapping, 192x144 for Head Banging, and 202x360 for Spinning. The maximum frame size remains at 1280x720 for all behaviors. The average frame sizes are 640.11x449.33 for Arm Flapping, 655.8x466.4 for Head Banging, and 500.9x396.0 for Spinning.

The SSBD dataset has an average video duration of 7.08 seconds for Arm Flapping, 11.79 seconds for Head Banging, and 17.22 seconds for Spinning.

Fig 3 shows the frames of the data set after applying YOLOv7 and masking, and Figs 4 5 6 show the frames of the data set after applying video augmentations.

### 3.2.1 YOLOv7 [31] Architecture Overview

YOLOv7 (You Only Look Once version 7) is a state-of-the-art deep learning model for real-time object detection. The architecture of YOLOv7 builds upon the innovations of previous YOLO versions, incorporating advancements to enhance accuracy, speed, and robustness. YOLOv7 maintains the fundamental design principles of the YOLO family while integrating several novel techniques to improve performance.

#### Fundamental Architecture

YOLOv7, like its predecessors, is an end-to-end single neural network architecture that predicts bounding boxes and class probabilities directly from full images in one evaluation. This design contrasts with other

detection systems where a preselected set of regions is processed. The architecture of YOLOv7 is designed to be fast and efficient, suitable for real-time applications.

### **Backbone: CSPDarknet**

The backbone of YOLOv7 is based on a modified version of the CSPDarknet53, a network known for its balance between efficiency and accuracy. The CSP (Cross-Stage Partial Network) structure reduces the redundancy in feature map computation, enhancing the learning capability and the inference speed. The CSPDarknet in YOLOv7 has been adjusted to optimize computational efficiency and accommodate newer hardware capabilities.

### **Neck: Path Aggregation Network (PAN)**

Following the backbone, the network uses a Path Aggregation Network (PAN) that enhances the feature hierarchy by aggregating different scales through bottom-up and top-down pathways. This ensures rich semantic information at various resolution scales, which is crucial for detecting objects of different sizes more effectively.

### **Head: Detection Layers**

The detection head of YOLOv7 utilizes anchor boxes predefined at different scales to predict bounding boxes relative to these anchors. For each bounding box, the network predicts the center coordinates, dimensions, objectness score (the probability that a box contains an object), and class probabilities. The head processes multiple scales simultaneously, allowing for robust detection across a diverse set of object sizes.

### **Enhancements in YOLOv7**

**1. Automatic Bounding Box Clustering:** YOLOv7 automates the selection of anchor box sizes using k-means clustering on the training dataset, improving the alignment between the model's predictions and the typical object dimensions found in the specific data.

**2. EIoU (Eliminate Intersection Over Union):** YOLOv7 introduces the EIoU loss, which refines the traditional Intersection Over Union (IoU) loss used in bounding box regression. This new metric helps reduce the localization errors in object detection.

**3. Mosaic and MixUp Data Augmentation:** YOLOv7 employs advanced data augmentation strategies like Mosaic and MixUp to enhance the diversity of training examples and improve model generalization. Mosaic combines four training images into a single one, while MixUp blends two images linearly.

**4. CmBN (Cross Mini-Batch Normalization):** The architecture uses a novel batch normalization technique, CmBN, which stabilizes training in smaller batch sizes by normalizing across multiple mini-batches.

**5. SPP (Spatial Pyramid Pooling):** The inclusion of SPP layers allows the network to maintain spatial hierarchies, providing robustness against object scale variations.

### **Training and Inference**

Training YOLOv7 involves using stochastic gradient descent (SGD) or Adam optimization with a specific focus on fine-tuning learning rates, weight decay, and other hyperparameters for optimal convergence. During inference, YOLOv7 employs non-maximum suppression (NMS) to refine the detection bounding boxes, ensuring that each detected object is represented by the most accurate bounding box.

YOLOv7's architecture represents a significant advancement in the field of real-time object detection. It successfully balances speed, accuracy, and the ability to run on various hardware platforms, making it suitable for a wide range of applications from autonomous vehicles to surveillance systems. Its comprehensive design improvements over prior models make it a formidable choice in the competitive landscape of object detection algorithms.

### **Handling Multiple Detections in YOLOv7**

In object detection tasks, especially in crowded scenes, it is common for the detection model to identify multiple bounding boxes around objects of interest. In the context of using YOLOv7 for object detection, my approach prioritizes the largest object in view, based on the area of the detected bounding boxes. This strategy is particularly useful in scenarios where the size of the object correlates with its importance or



relevance to the task.

### Selection of the Largest Bounding Box

During the detection phase, after the model predicts bounding boxes for objects in a frame, the following steps are implemented to select the largest box:

**1. Detection and Area Calculation:** For each frame processed by YOLOv7, all detected bounding boxes along with their class probabilities and objectness scores are evaluated. The area of each bounding box is calculated using the formula:  $\text{Area} = (x2 - x1) \times (y2 - y1)$  where  $x1$ ,  $y1$  and  $x2$ ,  $y2$  are the coordinates of the top-left and bottom-right corners of the bounding box, respectively.

**2. Identifying the Maximum Area:** Among all detected boxes, the one with the maximum area is selected. This selection is based on the assumption that larger objects are of higher priority:

---

#### Algorithm 1 Selecting the Largest Detected Bounding Box

---

```

1:  $max\_area \leftarrow 0$ 
2:  $max\_box \leftarrow None$ 
3: for each detection  $d$  in detections do
4:    $xyxy \leftarrow d.bbox$  ▷ Bounding box coordinates
5:    $conf \leftarrow d.conf$  ▷ Confidence score
6:    $cls \leftarrow d.cls$  ▷ Class identifier
7:    $area \leftarrow (xyxy[2] - xyxy[0]) \times (xyxy[3] - xyxy[1])$  ▷ Calculate area
8:   if  $area > max\_area$  then
9:      $max\_area \leftarrow area$ 
10:     $max\_box \leftarrow xyxy$ 
11:   end if
12: end for

```

---

**3. Cropping the Largest Box:** Once the largest bounding box is identified, it is cropped from the frame. This cropped region can then be processed further or used as the output, depending on the specific requirements of the application.

### Application and Implications

This methodology is particularly beneficial in applications where the focus is on identifying and tracking the most significant object in a scene, such as in surveillance systems where tracking the largest visible person might be crucial, or in traffic monitoring where larger vehicles might require more immediate attention.

#### Benefits

**Simplicity and Efficiency:** This approach is computationally efficient as it does not require complex post-processing of all detected objects.

**Focus on Relevant Objects:** By focusing on the largest object, the model ensures that smaller, potentially less relevant detections do not distract from the primary object of interest.

#### Limitations

**Oversight of Smaller Objects:** This method may overlook smaller, yet important, objects in the scene, which might be crucial depending on the application.

**Dependence on Scene Composition:** The effectiveness of this method may vary dramatically with different scene compositions or object distributions.

### Detailed Explanation of Masking in Object Detection

#### Introduction to Masking

In computer vision, masking refers to the process of isolating a specific part of an image or video frame to focus processing on that area. In the context of object detection using the YOLOv7 model, masking is used to highlight or process only the detected objects, specifically the largest object detected in the video frame as per the defined criteria.

## Implementation of Masking

After detecting objects in each frame, the algorithm isolates the largest object detected by applying a mask. This is achieved through the following steps:

**1. Initialization:** A mask is created with the same dimensions as the input frame but contains only zeros. This mask is essentially a binary image where the pixels of interest (i.e., those that belong to the largest detected object) will be set to a high value (255 in this case, representing white), and all other pixels will remain at zero (black).

**2. Drawing the Rectangle:** Once the bounding box with the maximum area is determined (i.e., the largest object), a rectangle is drawn on the mask. The coordinates of this rectangle correspond to the bounding box of the largest object. The rectangle is filled completely (denoted by -1 in the thickness parameter), turning the area inside the bounding box white.

**3. Applying the Mask:** The mask is then applied to the original frame to create a masked image. This step involves a bit-wise operation where the mask is used to keep the pixels within the bounding box unchanged, while all other pixels are turned to black. This highlights the largest detected object by masking out the rest of the frame.

### 4. Resizing

**Purpose of Resizing** Image resizing is a common preprocessing step in computer vision workflows, particularly in scenarios where uniform image sizes are required for further processing, visualization, or storage. Resizing the masked image standardizes the output, ensuring that each frame in the processed video maintains a consistent size, which is crucial for consistent visualization and could be beneficial for any subsequent analysis or machine learning tasks.

**Implementation of Resizing** After the masking step, where the largest detected object in each frame is highlighted, the masked image is resized to specific dimensions. This is implemented by the VideoMAE model. Here is the detailed breakdown of this step:

**Input:** masked image is the image obtained from the previous masking step, where the region outside the largest detected bounding box is blackened, focusing attention on the object.

**Target Size:** The target dimensions for the resizing are specified as (224, 224). This means the output image will be a square of 224 pixels by 224 pixels. Choosing a square shape can be particularly advantageous when dealing with data that will be input into neural networks that expect a fixed size and aspect ratio, or for creating uniformity in video frames for display purposes.

**Interpolation Method:** The '`interpolation=cv2.INTER_AREA`' parameter is critical for resizing. Interpolation methods determine how the pixel values are adjusted during resizing:

**INTER\_AREA:** This method is used for shrinking an image. It may be the preferred interpolation method when the goal is to reduce the resolution of an image while preserving the original appearance. It works by using pixel area relation, making it particularly suitable for making images smaller, as it can help avoid moiré patterns and maintain image quality.

## Benefits of Resizing in Object Detection

### Enhancement of Image Details

Resizing the masked images to a larger size, specifically to 720x720 pixels, serves a strategic purpose in scenarios where enhancing the visibility of details within the detected object is crucial. This approach is particularly valuable when the subsequent analysis requires a more granular examination of the object's features, which might be essential for accurate classification, detailed inspection, or precise monitoring tasks.

#### Explanation:

**Increased Resolution:** By enlarging the images, the approach leverages the higher pixel density to better capture and display finer details of the detected object. This is crucial when the object of interest contains features that are critical for further identification or analysis but might be lost at lower resolutions.

**Enhanced Visualization:** Larger images provide a clearer view when visually inspecting the details within the object. This can be especially beneficial for presentations or when manual verification steps are involved in the workflow.

**Improved Analytical Accuracy:** In applications involving detailed feature recognition, such as defect detection in manufacturing or intricate pattern recognition in wildlife monitoring, larger image sizes can allow algorithms to more accurately detect and classify subtle nuances.

**Trade-offs:** While resizing images to a larger size can enhance detail, it is important to acknowledge the trade-offs:

**Increased Computational Load:** Contrary to resizing for reduced dimensionality, increasing image size can lead to a higher computational burden. This requires more memory and processing power, which might affect the throughput of real-time systems.

**Potential Overfitting:** In machine learning scenarios, higher resolution images might lead to models focusing too much on minute, possibly irrelevant details, which can cause overfitting. It's essential to balance the level of detail with the generalizability of the model.

**5. Output:** The processed (masked and resized) image is then written to the output video file, ready for review or further analysis.

### Benefits of Masking in Object Detection

**Focus on Relevant Objects:** Masking allows for the isolation and focus on significant objects within a scene. In applications such as surveillance, traffic monitoring, or advanced research, focusing on the largest object could be critical for behavior analysis or event detection.

**Reduction of Noise:** By masking out irrelevant parts of the frame, the algorithm reduces the computational load for any subsequent processing and minimizes the noise that could interfere with the analysis.

**Enhanced Visualization:** Masking provides a clear visual representation of the detected object, which can be crucial for presentations, further manual assessments, or when visual outputs are necessary for decision-making processes.

### Video Augmentation Techniques applied on dataset

#### 1. Horizontal Flip

**Purpose:** Mirrors each frame of the video across the vertical axis. This augmentation helps in training models to recognize objects irrespective of their orientation, enhancing the robustness of object detection models.

**Implementation:** Utilizes `va.HorizontalFlip()` from the `vidaug` library, which applies a horizontal flip transformation to the video frames.

For a frame represented as a matrix  $F$ , the horizontal flip can be represented as:

$$F\_flipped(i, j) = F(i, W - j + 1)$$

Where  $W$  is the width of the frame,  $i$  ranges over the rows, and  $j$  ranges over the columns from 1 to  $W$ .

#### 2. Vertical Flip

**Purpose:** Mirrors each frame across the horizontal axis. Similar to horizontal flipping, vertical flipping helps models learn invariant features, useful in scenarios where vertical orientation can vary, such as aerial imagery analysis.

**Implementation:** Executed through `va.VerticalFlip()`, flipping the frames upside down.

For the vertical flip, the transformation can be represented as:

$$F\_flipped(i, j) = F(H - i + 1, j)$$

Where  $H$  is the height of the frame,  $i$  ranges over the rows from 1 to  $H$ , and  $j$  ranges over the columns.

#### 3. Upsample

**Purpose:** Increases the resolution of each frame by a specified scale factor. This is particularly useful for examining finer details within frames, which might be necessary for high-resolution applications or to test the performance of models at higher resolution levels.

**Implementation:** Each frame's dimensions are increased by a factor (e.g., 1.5 times the original size) using `cv2.resize` with `cv2.INTER_CUBIC` interpolation, which helps in preserving the smoothness of the image.

When upscaling a frame by a factor  $\alpha$ , the new dimensions are  $\alpha$  original dimensions. If  $F$  has dimensions  $W \times H$ , the upsample frame  $F'$  has dimensions:

$$W' = \alpha \times W, \quad H' = \alpha \times H$$

Interpolation is used to estimate pixel values in  $F'$ , typically using cubic interpolation:

$$F'(i, j) = \text{cubic\_interpolation} \left( F, \frac{i}{\alpha}, \frac{j}{\alpha} \right)$$

#### 4. Random Rotate

**Purpose:** Rotates each frame by a fixed angle (e.g., 25 degrees). Rotation augments are critical for training models to detect objects at various angles, enhancing detection accuracy in uncontrolled environments.

**Implementation:** The custom\_random\_rotate function uses OpenCV's `cv2.getRotationMatrix2D` and `cv2.warpAffine`, with the rotation center set to the frame's center and `cv2.BORDER_REFLECT101` to manage edge pixels.

For a rotation by angle  $\theta$ , the transformation matrix  $M$  can be given by:  $M = \begin{bmatrix} \cos \theta & -\sin \theta & 0 \\ \sin \theta & \cos \theta & 0 \\ 0 & 0 & 1 \end{bmatrix}$

A point  $(x, y)$  in the original frame is mapped to:  $\begin{bmatrix} x' \\ y' \\ 1 \end{bmatrix} = M \begin{bmatrix} x \\ y \\ 1 \end{bmatrix}$

Where  $(x', y')$  are the coordinates in the rotated frame.

#### 5. Invert Color

**Purpose:** Inverts the color of each frame. Color inversion is useful for testing models against unusual lighting conditions and color variability, ensuring robustness against diverse environmental conditions.

**Implementation:** This is achieved by subtracting each pixel value from 255 (i.e.,  $255 - \text{frame}$ ), effectively reversing the color spectrum.

The color inversion for a pixel value  $p$  in frame  $F$  can be represented as:  $F\_inverted(i, j) = 255 - F(i, j)$

#### 6. Downsample

**Purpose:** Reduces the frame rate of the video by a specified factor. Downsampling is used to simulate lower frame rate videos and to test the efficiency and effectiveness of models under reduced temporal resolution conditions.

**Implementation:** The function selectively writes frames to the output video based on the downsample factor; for instance, writing every second frame for a factor of 2.

If the original frame rate is  $R$  and the downsample factor is  $\beta$ , the new frame rate  $R'$  is:  $R' = \frac{R}{\beta}$

And frames are selected according to:  $F'(t) = F(\beta \times t)$

Where  $t$  is the frame index in the downsampled video.

These augmentations introduce variability into the dataset, which is essential for training robust machine learning models, particularly in object detection and video analysis tasks. By applying these transformations, models can be trained to perform well across a variety of real-world conditions, ensuring they are not only accurate but also versatile in handling different scenarios and challenges.

### 3.3 Proposed Methodology

This study uses videos to show how to recognize and classify human behavior using a robust deep learning model. Videos, on the other hand, are collections of images put in a certain order to create motion. For video categorization, a variety of techniques might be used. This study suggested using VideoMAE along with YOLOv7 and video augmentation. We provide a complete explanation of the essential elements included in our suggested models in the parts that follow, along with a detailed display of their architectural layouts.

#### 3.4 VideoMAE [29]

The intrinsic properties of video data, such as temporal redundancy—where successive frames often contain similar information—and temporal correlation—where events unfold over time—present unique opportunities and challenges for machine learning models. The Video Masked Autoencoder (VideoMAE) framework leverages these properties, utilizing a strategy adapted from successes in natural language processing (NLP)

and still image analysis, where masked autoencoders have demonstrated significant efficacy.

## VideoMAE Architecture

### Masking Strategy

- **Tube Masking:** Central to VideoMAE is its novel tube masking strategy, which applies a consistent mask across the temporal dimension of video clips. This approach ensures that if a segment is masked in one frame, the corresponding segments in adjacent frames are also masked. This strategy significantly increases the reconstruction challenge, preventing the model from merely interpolating spatially adjacent frames to fill in gaps, thus encouraging the learning of robust spatiotemporal features.

### Encoder-Decoder Model

- **Asymmetric Architecture:** VideoMAE adopts an asymmetric encoder-decoder architecture, common in masked autoencoder designs but tailored for video. The heavy encoder processes the unmasked frames, transforming them into a rich, compressed latent space. Conversely, the lightweight decoder aims to reconstruct the original full video from this compressed representation.
- **Vision Transformer (ViT):** Unlike many conventional video processing models that rely on 3D convolutions, VideoMAE utilizes a plain ViT, treating video frames as sequences of flattened 2D patches (tokens). This adaptation allows the model to leverage the powerful self-attention mechanisms of transformers, facilitating a global understanding of video content across both spatial and temporal dimensions.

## Methodology

### Self-Supervised Pre-training

- **Training Objective:** The model is trained in a self-supervised manner by predicting the video parts that are masked out, using only the visible segments. The objective is to minimize the difference between the reconstructed video and the original unmasked video, typically measured by a reconstruction error such as Mean Squared Error (MSE).
- **High Masking Ratio:** VideoMAE employs an unusually high masking ratio (up to 95%), a strategy made viable by the redundancy in video data. This extensive masking forces the model to infer significant portions of the video, enhancing its ability to learn predictive and generative video features without relying on vast amounts of labeled data.

```

VideoMAEForVideoClassification(
  (videomae): VideoMAEModel(
    (embeddings): VideoMAEEmbeddings(
      (patch_embeddings): VideoMAEPatchEmbeddings(
        (projection): Conv3d(3, 768, kernel_size=(2, 16, 16), stride=(2, 16, 16))
      )
    )
    (encoder): VideoMAEEncoder(
      (layer): ModuleList(
        (0-11): 12 x VideoMAELayer(
          (attention): VideoMAEAttention(
            (attention): VideoMAESelfAttention(
              (query): Linear(in_features=768, out_features=768, bias=False)
              (key): Linear(in_features=768, out_features=768, bias=False)
              (value): Linear(in_features=768, out_features=768, bias=False)
              (dropout): Dropout(p=0.0, inplace=False)
            )
            (output): VideoMAESelfOutput(
              (dense): Linear(in_features=768, out_features=768, bias=True)
              (dropout): Dropout(p=0.0, inplace=False)
            )
          )
          (intermediate): VideoMAEIntermediate(
            (dense): Linear(in_features=768, out_features=3072, bias=True)
            (intermediate_act_fn): GELUActivation()
          )
          (output): VideoMAEOutput(
            (dense): Linear(in_features=3072, out_features=768, bias=True)
            (dropout): Dropout(p=0.0, inplace=False)
          )
          (layernorm_before): LayerNorm((768,), eps=1e-12, elementwise_affine=True)
          (layernorm_after): LayerNorm((768,), eps=1e-12, elementwise_affine=True)
        )
      )
      (layernorm): LayerNorm((768,), eps=1e-12, elementwise_affine=True)
    )
    (classifier): Linear(in_features=768, out_features=3, bias=True)
  )
)

```

Fig. 7. VideoMAE Classifier Architecture

## 4 EXPERIMENTAL RESULT

The **High-Performance Computing (HPC) - SURYA** was used to train the model. The HPC infrastructure features 16 compute nodes, we utilized one HPC node equipped with 40 CPU cores, 2 NVIDIA V100 GPUs with 24GB RAM each, and 376GB of system RAM.

### 4.1 PERFORMANCE PARAMETERS

In the discipline of deep learning, a classification report serves as a statistical gauge of performance. Its goal is to show off the classification model’s accuracy, recall, F1 score, precision, and loss metrics. For multiclass classification sparse-categorical-cross-entropy loss function is used as a loss function.

**Accuracy:** The accuracy of a model is determined by dividing the total number of predictions by the number of accurate predictions it made. The formula to calculate accuracy is as follows:

$$Accuracy = \frac{\sum_{i=1}^N I(y_i - \hat{y}_i)}{N}$$

Where: N is the total number of data,  $y_i$  is true value of  $i^{th}$  data,  $\hat{y}_i$  is predicted value of  $i^{th}$  data.

**Recall:** It is the ratio of accurately recognized instances of a given class to the total number of actual instances of that class for that specific class.

$$Recall_{class\_i} = \frac{TP_{class\_i}}{TP_{class\_i} + FN_{class\_i}}$$

**Precision:** It is defined as the ratio of successfully recognized instances of a given class to all instances projected to belong to that class.

$$Precision_{class\_i} = \frac{TP_{class\_i}}{TP_{class\_i} + FP_{class\_i}}$$

**F1 score:** The F1 Score is a balance between precision and recall, calculated as the harmonic mean of the two. When there is an uneven distribution of classes, it is very useful.

$$F1\ Score_{class\_i} = 2 \times \frac{Precision_{class\_i} \times Recall_{class\_i}}{Precision_{class\_i} + Recall_{class\_i}}$$

**Loss:** The sparse-categorical-crossentropyloss function is best-suited loss function for multiclass classification. The negative log-likelihood of the expected probability of the true class is the loss for a single observation. The average of the various losses is the overall loss over the whole dataset (or over a batch during training):

$$Sparse\_Categorical\_Crossentropy = -\frac{1}{N} \sum_{i=1}^N \log(p_{i,y_i})$$

### 4.2 Ablation Studies

In our research, we conducted an ablation study to assess the impact of different hyperparameters on model performance. By systematically varying batch size, split ratio, and learning rate, we were able to evaluate their individual contributions to the overall effectiveness of the model. This analysis enabled us to identify optimal configurations, thus refining the model’s performance and ensuring more robust and accurate results. The insights gained from this study were crucial for optimizing the model’s architecture and guiding its further development.



#### 4.2.1 For variation in Learning Rate On original SSBD data

The table 3 presents the training time and performance metrics of the VideoMAE model across various learning rates, highlighting the relationship between these parameters. As the learning rate decreases from 0.01 to 0.0001, a notable trend emerges: training time decreases significantly while accuracy improves, peaking at 0.58 with a learning rate of 0.0001. This rate also yields the highest precision at 0.81, indicating a strong ability to correctly identify relevant instances. In contrast, the learning rates of 0.01 and 0.001 show lower accuracy and precision, with longer training times of 16 hours and 15.1 hours, respectively. The learning rate of 0.00001, while still efficient in training time (5.2 hours), demonstrates a slight drop in both accuracy (0.5) and precision (0.46). Overall, the findings suggest that a careful selection of the learning rate is essential for optimizing the model's performance, balancing accuracy, precision, and training efficiency.

**Table 3.** Training Time of VideoMAE model with variation in learning rate

Learning Rate	Training Time	Accuracy	Precision	Recall	F1 Score
0.01	16 h	0.33	0.22	0.33	0.26
0.001	15.1 h	0.33	0.22	0.33	0.26
0.0001	5.3 h	0.58	0.81	0.58	0.56
0.00001	5.2 h	0.5	0.46	0.5	0.44

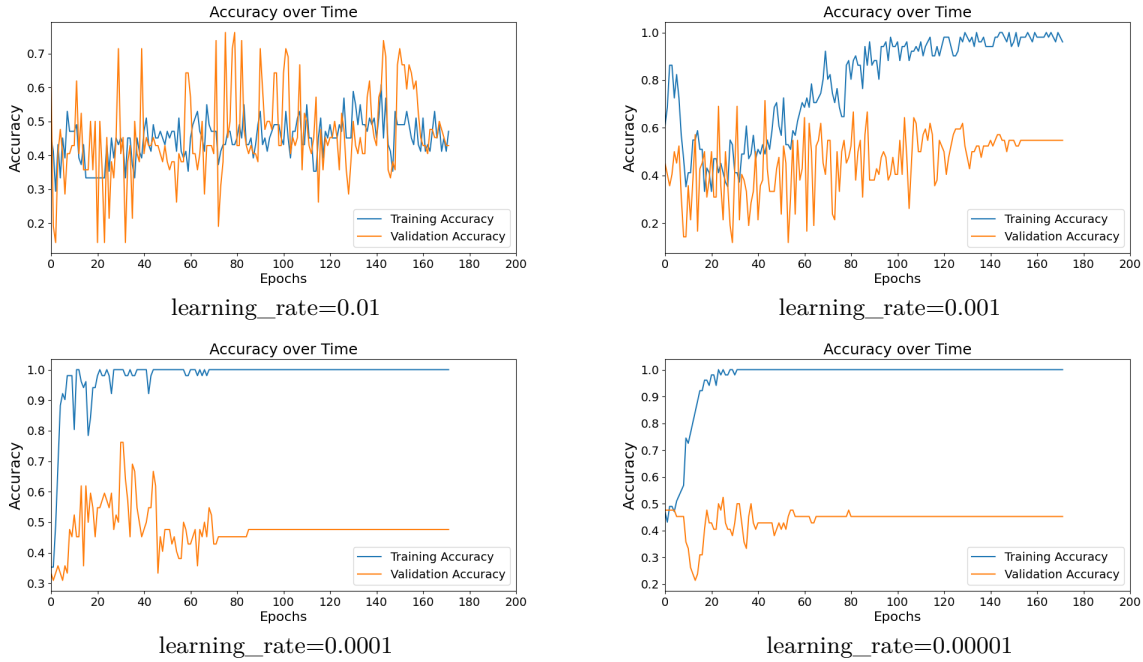


**Fig. 8.** Comparison of Accuracy for various learning rate

Figure 8 illustrates the impact of varying learning rates on the training and validation accuracy of a model over 200 epochs. The graphs depict four different learning rates: 0.01, 0.001, 0.0001, and 0.00001. At a learning rate of 0.01, both training and validation accuracies fluctuate significantly, indicating instability and potential overfitting. In contrast, a learning rate of 0.001 shows a more stable increase in training accuracy while validation accuracy remains lower, suggesting some overfitting. The learning rate of 0.0001 achieves high training accuracy quickly, but validation accuracy remains lower, indicating overfitting. Finally,

a learning rate of 0.00001 demonstrates a stable and rapid convergence in training accuracy with a moderate increase in validation accuracy, suggesting a balanced learning process. These observations underscore the importance of selecting an appropriate learning rate to optimize model performance and generalization.

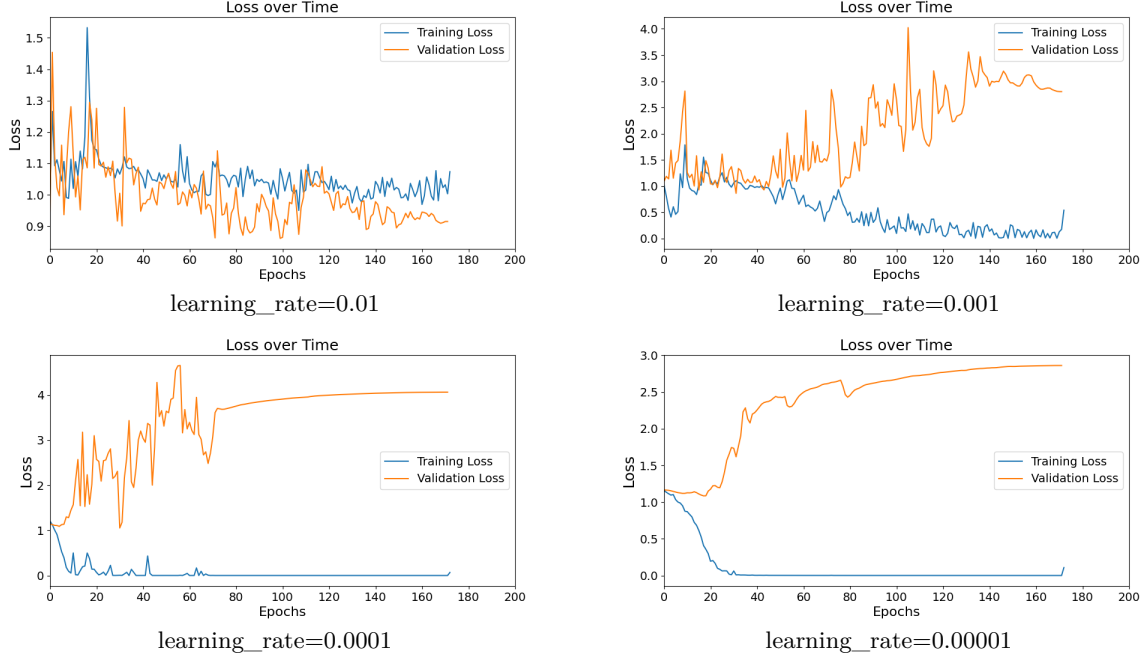


**Fig.9.** Comparison of Loss for various learning rate

Figure 9 presents the effect of different learning rates on the training and validation loss of a model over 200 epochs. The graphs show four distinct learning rates: 0.01, 0.001, 0.0001, and 0.00001. At a learning rate of 0.01, both training and validation losses demonstrate instability with frequent fluctuations, indicating potential overfitting. For a learning rate of 0.001, training loss decreases steadily while validation loss remains higher, suggesting overfitting issues. With a learning rate of 0.0001, training loss quickly approaches zero, whereas validation loss stays relatively high, again indicating overfitting. Lastly, a learning rate of 0.00001 reveals a smooth and rapid decline in training loss with consistent performance, though the validation loss remains constant and higher, suggesting underfitting. These results highlight the critical role of learning rate selection in achieving optimal model convergence and minimizing loss.

#### 4.2.2 For variation in Batch Size On Original SSBD data

The table4 summarizes the training time and performance metrics of the VideoMAE model with varying batch sizes, illustrating the impact of batch size on model efficiency and effectiveness. As the batch size increases from 2 to 4, there is a significant improvement in accuracy, which rises to 0.83 with a training time of 5.3 hours. This batch size also achieves high precision at 0.88, indicating a strong performance in correctly identifying relevant instances. However, when the batch size is increased further to 8 and 16, the accuracy declines to 0.66, with precision values of 0.63 and 0.74, respectively, despite maintaining the same training time of 4.5 hours. The recall and F1 scores also reflect this trend, emphasizing that while larger batch sizes can enhance training speed, they may compromise the model's ability to generalize effectively. Overall, these findings suggest that a batch size of 4 is optimal for balancing training time and model performance, yielding the best accuracy and precision for the VideoMAE model.

**Table 4.** Training Time of VideoMAE model with variation in learning rate

Batch Size	Training Time	Accuracy	Precision	Recall	F1 Score
2	6.2 h	0.5	0.64	0.5	0.44
4	5.3 h	0.83	0.88	0.83	0.82
8	4.5 h	0.66	0.63	0.66	0.62
16	4.5 h	0.66	0.74	0.66	0.65

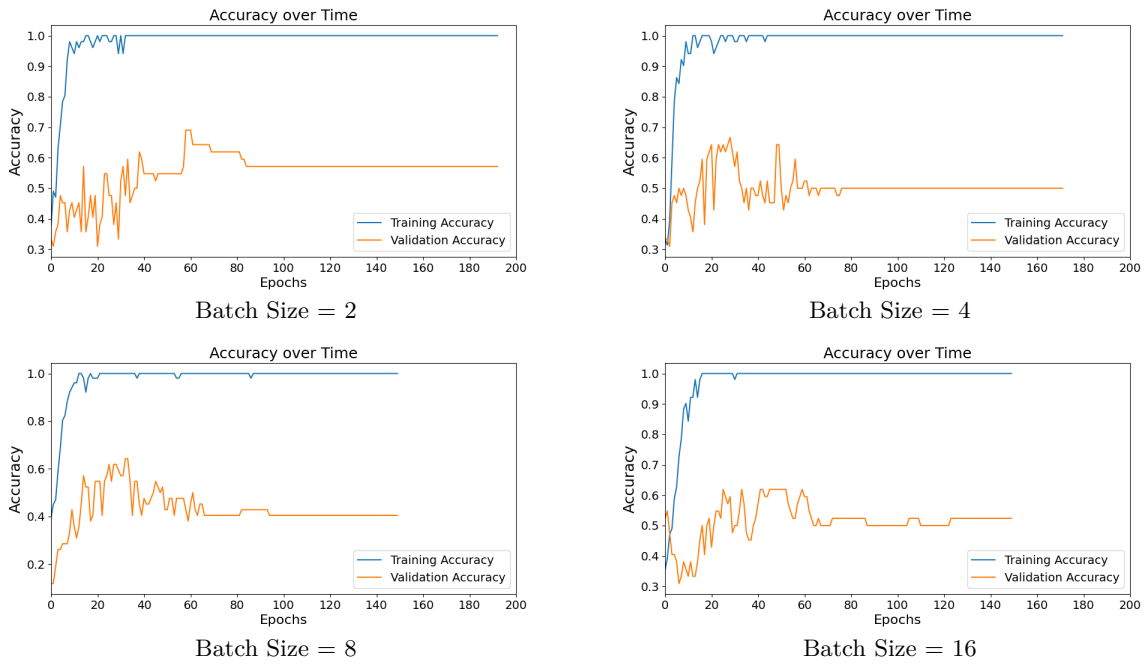
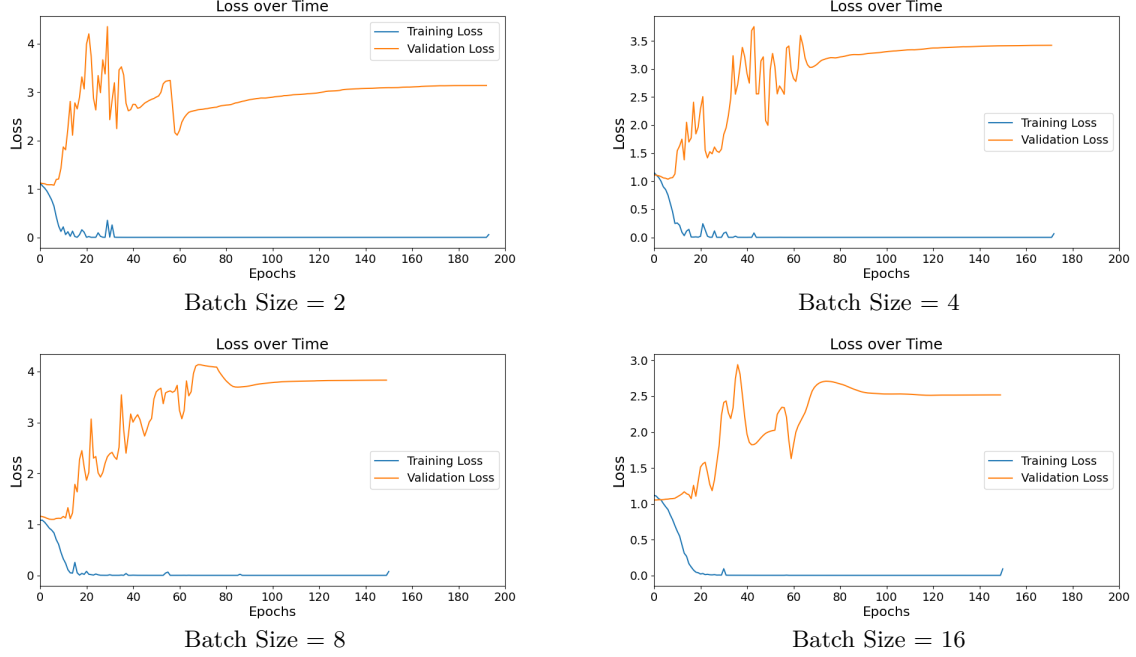
**Fig. 10.** Comparison of Accuracy for various batch size

Figure 10 illustrates the impact of different batch sizes on the training and validation accuracy of a model over 200 epochs, using batch sizes of 2, 4, 8, and 16. Across all batch sizes, training accuracy rapidly reaches high levels, while validation accuracy remains significantly lower, indicating potential overfitting. With smaller batch sizes (2 and 4), there is a noticeable fluctuation in validation accuracy, suggesting instability during training. As the batch size increases to 8 and 16, validation accuracy stabilizes but does not improve significantly, still indicating overfitting. We selected a batch size of 4 for our experiments. We keep batch size low during machine learning model training to address memory constraints, especially on hardware like GPUs with limited memory. Smaller batch sizes also help models generalize better by introducing more noise into gradient estimates, which can prevent overfitting. Additionally, lower batch sizes enable more frequent updates to the model's parameters, potentially leading to faster convergence. However, there is a trade-off between computation efficiency and model performance, so selecting an optimal batch size is crucial.



**Fig. 11.** Comparison of Loss for various batch size

Figure 11 presents the effect of different batch sizes on training and validation loss over 200 epochs, with batch sizes of 2, 4, 8, and 16. Across all batch sizes, training loss rapidly decreases and stabilizes at a low level, indicating effective learning. However, validation loss remains high and relatively constant, suggesting overfitting. Smaller batch sizes, such as 2 and 4, show greater fluctuations in validation loss, reflecting instability. As batch size increases to 8 and 16, the validation loss becomes more stable, but without significant improvement. This behavior highlights the trade-off between computational efficiency and model generalization. Selecting an optimal batch size is crucial, as smaller sizes may introduce beneficial noise to gradient estimates, aiding generalization, while larger sizes enhance stability but may not address overfitting efficiently.

#### 4.2.3 For Variation in Split Ratio On Original SSBD data

The table5 presents the training time and performance metrics of the VideoMAE model based on different data split ratios, highlighting how the division of training, validation, and test sets affects model efficiency and effectiveness. The split ratio of 60:20:20 results in a training time of 5.6 hours, yielding an accuracy of 0.53, which indicates limited model performance. In contrast, the 70:15:15 split significantly enhances the model's performance, achieving an accuracy of 0.83 alongside high precision at 0.88, suggesting a robust capability in correctly identifying relevant instances. However, the 80:10:10 split, while resulting in a slightly longer training time of 5.9 hours, shows a decrease in accuracy to 0.66, with precision remaining at 0.66. The recall and F1 scores reflect similar trends, emphasizing that the choice of data split ratio can substantially influence model outcomes. Overall, these results suggest that a 70:15:15 split ratio is optimal for achieving a balance between training time and performance metrics, particularly accuracy and precision, for the VideoMAE model.

**Table 5.** Training Time of VideoMAE model with variation in learning rate

Split Ratio	Training Time	Accuracy	Precision	Recall	F1 Score
60:20:20	5.6 h	0.53	0.5	0.53	0.50
70:15:15	5.3 h	0.83	0.88	0.83	0.82
80:10:10	5.9 h	0.66	0.66	0.66	0.65

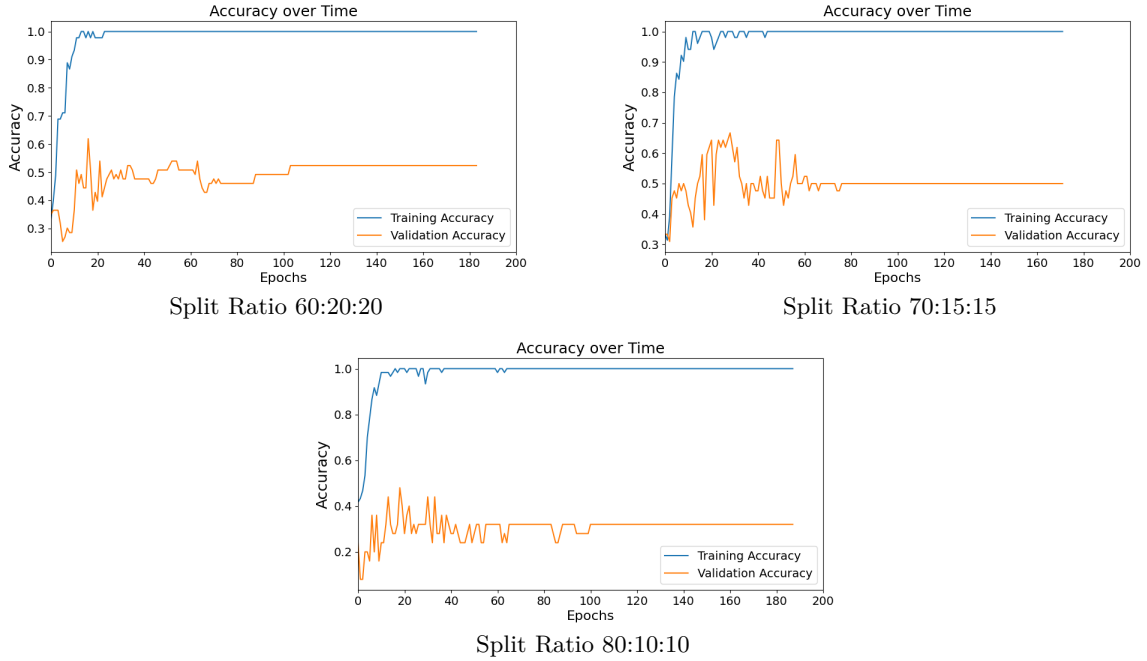
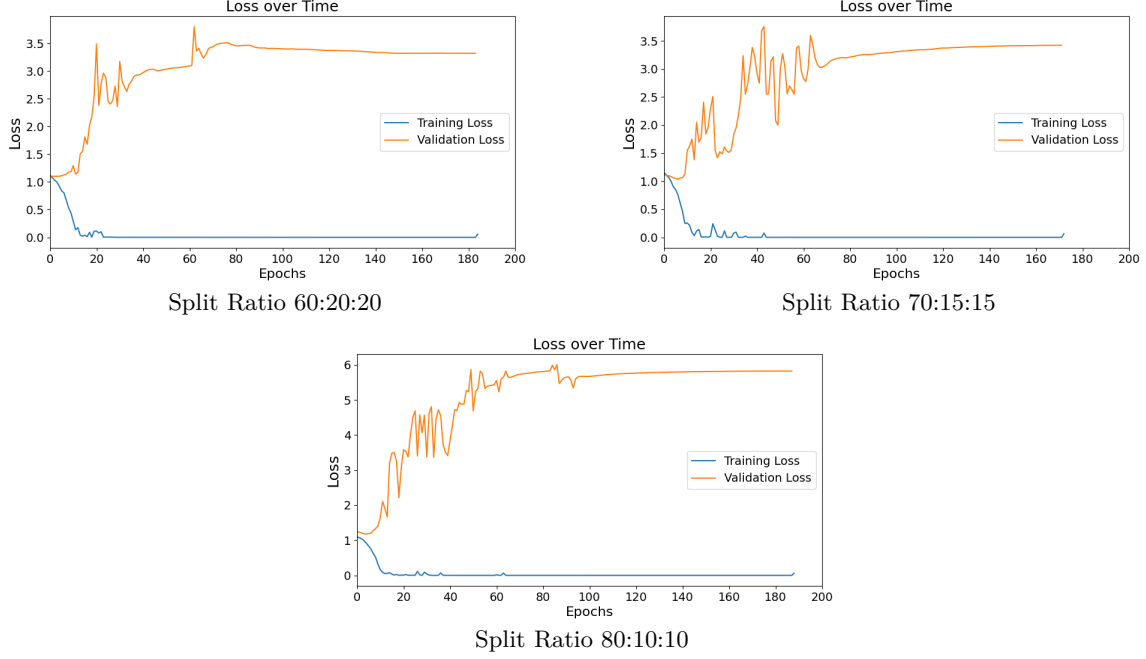
**Fig. 12.** Comparison of Accuracy for various Split Ratio

Figure 12 illustrates the impact of different data split ratios on training and validation accuracy over 200 epochs, using splits of 60:20:20, 70:15:15, and 80:10:10. In all scenarios, training accuracy quickly reaches high levels, suggesting effective learning. However, validation accuracy remains lower across all splits, indicating possible overfitting. The 60:20:20 split shows more fluctuation in validation accuracy, reflecting variability. The 70:15:15 split offers a slightly more stable validation accuracy, while the 80:10:10 split shows consistent but lower validation accuracy, suggesting that a larger training set may improve learning but can also exacerbate overfitting if not balanced well. These results underscore the importance of choosing an appropriate data split to balance training efficiency and model generalization.



**Fig. 13.** Comparison of Loss for various Split Ratio

Figure 13 depicts the effect of different data split ratios on training and validation loss over 200 epochs, using splits of 60:20:20, 70:15:15, and 80:10:10. In each scenario, training loss rapidly decreases and stabilizes at a low level, indicating effective learning. However, validation loss remains high and relatively stable, suggesting overfitting. The 60:20:20 split shows higher fluctuations in validation loss, indicating instability. The 70:15:15 split offers slightly more stable validation loss, while the 80:10:10 split maintains consistent but elevated validation loss, suggesting that increasing the training set size may improve model learning but could also exacerbate overfitting if not balanced correctly. These observations highlight the importance of selecting an appropriate data split to optimize model performance and generalization.

### 4.3 Results and Analysis

The SSBD dataset consists of total 75 videos, 25 video of each class. We randomly divide the dataset into training, testing and validation in the ratio of 70:15:15. Further, to validate the model at the time of training this 15% validation data is used. Training data has 17 videos of arm flapping, 17 videos of head banging, and 17 videos of spinning class. Testing data has 4 videos of arm flapping, 4 videos of head banging, and 4 videos of spinning class. Validation data has 4 videos of arm flapping, 4 videos of head banging, and 4 videos of spinning class.

The trim\_SSBD dataset consists of total 124 videos. We randomly divide the dataset into training, testing and validation in the ratio of 70:15:15. Further, to validate the model at the time of training this 15% validation data is used. Training data has 20 videos of arm flapping, 28 videos of head banging, and 37 videos of spinning class. Testing data has 5 videos of arm flapping, 7 videos of head banging, and 9 videos of spinning class. Validation data has 4 videos of arm flapping, 6 videos of head banging, and 8 videos of spinning class.

The trim\_SSBD\_yolo\_augment dataset consists of total 868 videos. We randomly divide the dataset into training, testing and validation in the ratio of 70:15:15. Further, to validate the model at the time of training this 15% validation data is used. Training data has 142 videos of arm flapping, 200 videos of head banging, and 264 videos of spinning class. Testing data has 31 videos of arm flapping, 44 videos of head banging, and 57 videos of spinning class. Validation data has 30 videos of arm flapping, 43 videos of head banging, and 57 videos of spinning class.

**Table 6.** Class-wise Results of VideoMAE model on Original SSBD data

Class	Accuracy	Precision	Recall	F1 Score
ArmFlapping	1.0	1.0	1.0	1.0
HeadBanging	0.5	1.0	0.5	0.66
Spinning	1.00	0.66	1.00	0.8

**Table 7.** Class-wise Results of VideoMAE model on trimmed SSBD data

Class	Accuracy	Precision	Recall	F1 Score
ArmFlapping	0.4	0.4	0.4	0.4
HeadBanging	0.28	0.5	0.28	0.36
Spinning	1.0	0.75	1.0	0.85

**Table 8.** Class-wise Results of VideoMAE on trim\_SSBD+yolov7 data

Class	Accuracy	Precision	Recall	F1 Score
ArmFlapping	0.6	1.0	0.6	0.75
HeadBanging	0.85	0.75	0.85	0.8
Spinning	1.0	0.9	1.0	0.94

**Table 9.** Class-wise Results of VideoMAE on SSBD+Yolov7+Augmentation data

Class	Accuracy	Precision	Recall	F1 Score
ArmFlapping	0.93	1.0	0.93	0.96
HeadBanging	0.97	0.97	0.97	0.97
Spinning	1.0	0.96	1.0	0.98

The tables 6 7 8 9 present class-wise performance metrics—accuracy, precision, recall, and F1 score—of the VideoMAE model evaluated on different SSBD datasets. Initially, on the Original SSBD data, "ArmFlapping" achieves perfect scores across all metrics, while "HeadBanging" shows lower recall and F1 score, indicating misclassification. "Spinning" maintains high recall but lower precision. Trimmed SSBD data shows a decrease in "ArmFlapping" and "HeadBanging" performance, with "Spinning" remaining stable. The trim\_SSBD+yolov7 dataset improves "ArmFlapping" and "HeadBanging" metrics, with "Spinning" achieving high scores. Finally, the SSBD+Yolov7+Augmentation dataset shows marked improvement, with "ArmFlapping" and "HeadBanging" nearing perfect scores and "Spinning" achieving excellent metrics. These results highlight the positive impact of data trimming, model refinement, and augmentation on classification performance.

**Table 10.** Over All Results of VideoMAE

Data Set	Accuracy	Precision	Recall	F1 Score	training time
SSBD	0.83	0.88	0.83	0.82	5.2 hour
trim_SSBD	0.61	0.54	0.56	0.54	8.9 hour
trim_SSBD_yolo	0.85	0.88	0.81	0.83	7.5 hour
trim_SSBD_yolo_augment	0.97	0.98	0.97	0.97	51.1 hour



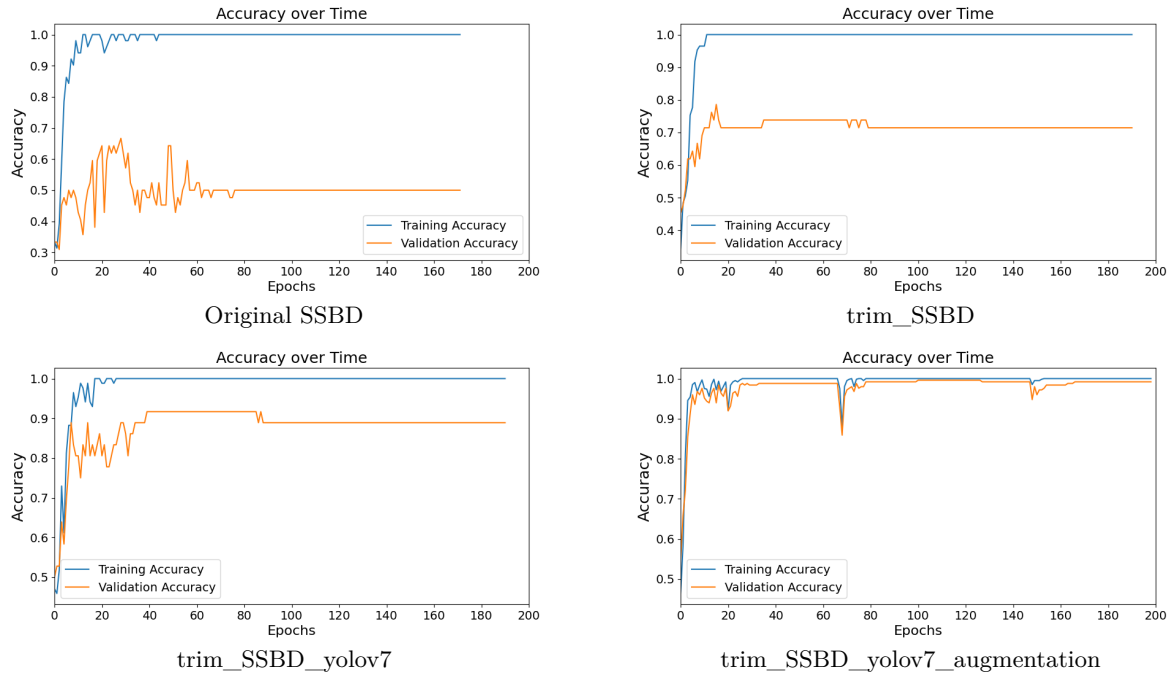


Fig. 14. Comparison of Accuracy

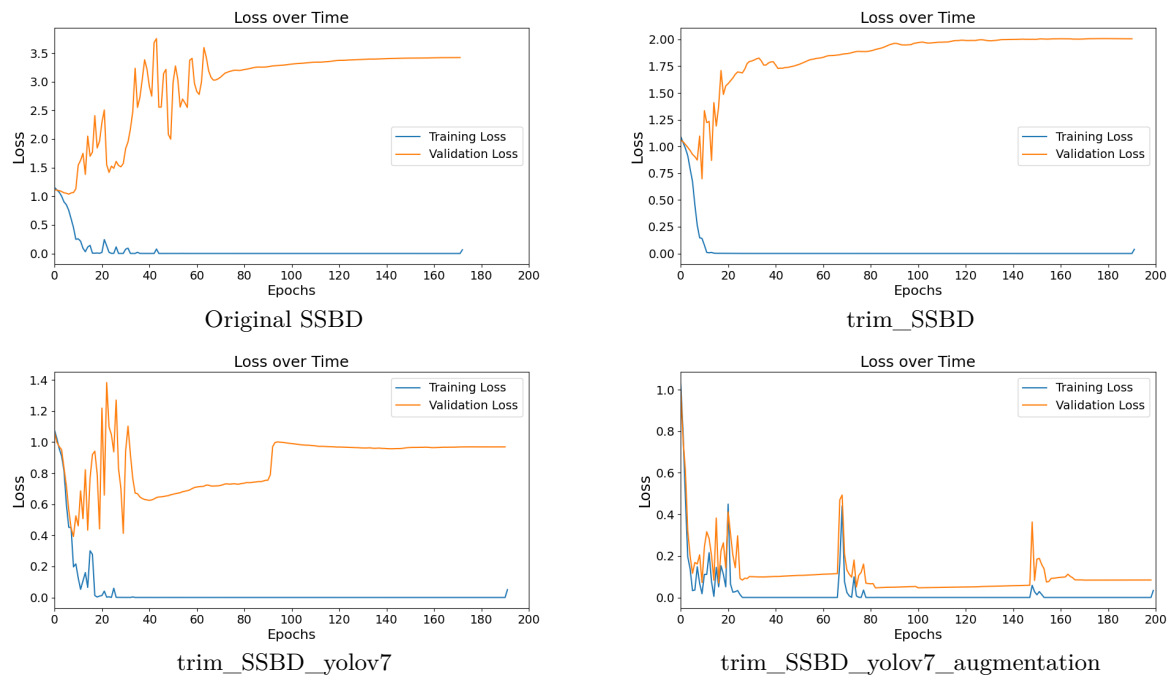


Fig. 15. Comparison of Loss

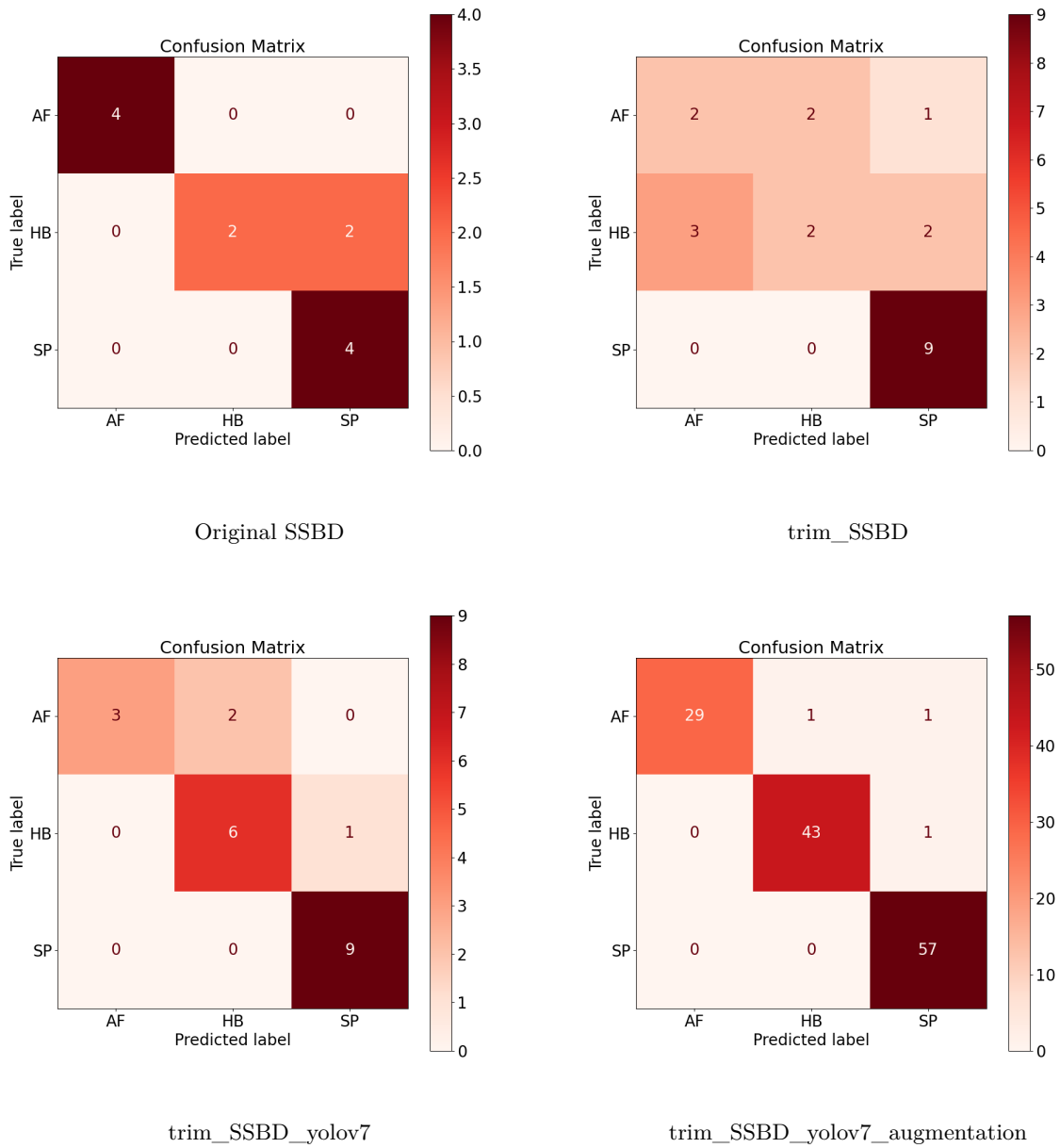
**Fig. 16.** Comparison of Confusion Matrices

Table 10 Shows the class-wise results of the VideoMAE model. The model scored best for the data trim\_SSBD\_yolo\_augment with an F1 score of 0.97, a precision of 0.98, and a recall of 0.97. The overall test accuracy achieved by the model is 97% with a loss of 0.173. The VideoMAE model was trained on 200 epochs using learning rate of 0.00005, batch size 4 and split ratio 70:15:15. The model achieved 100% training and 99.1% validation accuracy. The Fig 14 15 describes the model training and validation accuracy and loss.

Figure 16 presents a comparison of confusion matrices for Original SSBD, trim\_SSBD, trim\_SSBD\_yolov7, and trim\_SSBD\_yolov7 with augmentation. Each matrix shows true labels on the vertical axis and predicted labels on the horizontal axis for classes AF, HB, and SP. In the Original SSBD, predictions are relatively dispersed, indicating misclassification across all classes. The trim\_SSBD model shows slight improvement but still struggles with accurate predictions. The trim\_SSBD\_yolov7 matrix demonstrates better

classification accuracy, with more correctly predicted instances along the diagonal. The trim\_SSBD\_yolov7 with augmentation further enhances performance, showing the highest concentration of correct predictions, particularly in class SP. These matrices highlight the effectiveness of model refinement and data augmentation in improving classification accuracy.

Due to its dependence on human behavior and the need for extensive observation, stereotypical repeated gesture is a challenging task. To categorize autistic children's repetitive gestures via videos, this research study used a yolov7 with transformer based VideoMAE model. The foundation of this system is computer vision, deep learning, and a transformer. When compared to existing techniques, the accuracy of the proposed models is greater. Arm flapping, head banging, and spinning were the three types of repeated gestures that our video classification models were trained on. The videos were taken out of the SSBD [26].

This work has the benefit of being built on algorithms that can extract features from video clips in real-time, including the VideoMAE model. Furthermore, the test video might be recorded when the child is engaged in typical activities in an unrestricted regular setting. It is well established that children with ASD dislike the limitations and procedures of structured examinations. In addition, there is an option to observe the outcome immediately without using statistical analyzes or translating the video into a different format, which might be difficult for psychologists to understand.

#### 4.4 Result Comparison with state of the art

**Table 11.** A comparative analysis of the proposed model against prior studies on the SSBD dataset, focusing on accuracy and F1-score metrics.

Model	Method	Results
Rajagopalan et al. [26]	Bag Of Words (BOW)	50.7% accuracy
Rajagopalan et al. [27]	Histogram of Dominant Motions (HDM)	76% accuracy
Lakkapragad et al. [18]	MobileNetV2, LSTM	F1 score of .84 Precision .89 Recall .80
Dia et al. [13]	3D Convnet and Multi-Stage Temporal Convolutional Network	74.5% accuracy 0.73 F1-Score 0.73 Recall
Ali et al. [3]	Yolov5, DeepSORT, RAFT	75% accuracy 0.90 F1 Score
<b>Our Work</b>	Yolov7, Augmentations, VideoMAE	<b>97% accuracy</b> <b>.98 precision</b> <b>.97 F1 score</b> <b>0.97 recall</b>

When the proposed model was compared to Lakkapragad et al. [18], the suggested models outperformed the previous models, which input the hand landmarks into an LSTM and MobileNetV2 using MediaPipe to extract them. An F1 score of 84.0 was attained by their model. In this work, Lakkapragad et al. [18] only work with the Arm flapping class. The histogram of dominating motion and Bag of words was combined with the optical flow histogram by Rajagopalan et al. [26,27]. Their classification model distinguished between headbanging, spinning, and hand flapping in three groups with an accuracy of 76.3%. ASD and hand flapping were investigated from all three classes by Ali et al. [3]. Using a large collection of videos depicting the stereotyped behavior of children, Ali et al. [3] investigated the identification of ASD behavior. Their combination of an RGB and optical flow two-stream I3D model produced an accuracy of 75%. Negin

F et al. [25] collected a new dataset and recognized autistic and non-autistic children via vision assistance. Multiple models such as LSTM, ConvLSTM, and 3DCNN have been implemented and achieved an accuracy of 79%. 3D CNN and Multi-stage temporal convolution network were implemented by Dia et al. [13] on modified SSBD with all three classes. Dia et al. [13] got 61 videos out of 75 videos from SSBD and collected more videos and generated a performance of 83% accuracy. There is a comparative analysis in Table 11.

We discovered that the VideoMAE models excel primarily due to their innovative use of masked autoencoding, which leverages the inherent redundancy in video data to enhance learning efficiency. By masking a substantial portion of the video frames—up to 90-95%—these models focus on reconstructing the missing content, which compels them to capture the essential temporal and spatial dynamics of the videos. This method of forcing the model to predict large unseen segments encourages a deeper understanding of video content, helping the model learn robust, high-level features that are critical for interpreting complex video sequences. The separation of the encoder and decoder in the VideoMAE architecture allows for processing efficiency, as the encoder handles only the unmasked frames, significantly reducing the computational load. Moreover, this setup minimizes overfitting, as the model must generalize well to perform accurate reconstruction across varied inputs. Such characteristics make VideoMAE particularly effective for self-supervised pre-training on large, unlabeled video datasets, facilitating superior performance on a range of video understanding tasks once fine-tuned.

## 5 Conclusion

In this study, behaviors from videos are analyzed using deep learning and computer vision to classify stereotypical repetitive gestures. We trained our models using videos of children going about their everyday lives in an uncontrolled environment to predict repetitive movements. The videos included three different types of videos: arm flapping, head banging, and spinning. The testing set yielded an 95% score for the VideoMAE model.

We used the VideoMAE model and the insights from our trained models to create a video-based repetitive behavior analysis, which can help parents and psychologists in the future to diagnose aberrant behaviors like arm flapping, head banging, and spinning repetitive gestures which may be an indication of autism. This will increase the study's usefulness and practical applicability. Our objective is to advance the detection of repetitive movements in autistic children by using these contemporary technological advancements, enabling early intervention and subsequent therapy for children.

As a result, this may help autistic children with early detection of gestures and become more adept at social communication, which would lessen the challenges that their families face.

The proposed VideoMAE model provides strong capabilities for detecting repetitive autistic gestures. Repetition in gestures needs to extract spatial as well as temporal features. The VideoMAE model is effective in extracting both spatial and temporal information through its masked autoencoders and attention mechanisms, comparing subsequent frames and detecting repetitive movements in a video. Our findings show that the proposed model is capable of successfully recognizing behavioral patterns in uncontrolled, real-world videos. One of the study's future objectives is the potential for high-quality video collations, which would increase the classification findings' accuracy.

## Acknowledgment

The authors are grateful to the Ministry of Human Resource and Development and the Indian Institute of Information Technology, Allahabad for supplying the necessary materials required to complete this work.

## References

1. Akter, T., Ali, M.H., Khan, M., Satu, M., Uddin, M., Alyami, S.A., Ali, S., Azad, A., Moni, M.A., et al.: Improved transfer-learning-based facial recognition framework to detect autistic children at an early stage. *Brain Sciences* **11**(6), 734 (2021)
2. Akter, T., Satu, M.S., Khan, M.I., Ali, M.H., Uddin, S., Lio, P., Quinn, J.M., Moni, M.A.: Machine learning-based models for early stage detection of autism spectrum disorders. *IEEE Access* **7**, 166509–166527 (2019)

3. Ali, A., Negin, F.F., Bremond, F.F., Thümmmler, S.: Video-based behavior understanding of children for objective diagnosis of autism. In: VISAPP 2022-17th International Conference on Computer Vision Theory and Applications (2022)
4. Almuqhim, F., Saeed, F.: Asd-saenet: a sparse autoencoder, and deep-neural network model for detecting autism spectrum disorder (asd) using fmri data. *Frontiers in Computational Neuroscience* **15**, 27 (2021)
5. Alsaade, F.W., Alzahrani, M.S.: Classification and detection of autism spectrum disorder based on deep learning algorithms. *Computational Intelligence and Neuroscience* **2022** (2022)
6. Arora, N.K., Nair, M., Gulati, S., Deshmukh, V., Mohapatra, A., Mishra, D., Patel, V., Pandey, R.M., Das, B.C., Divan, G., et al.: Neurodevelopmental disorders in children aged 2–9 years: Population-based burden estimates across five regions in india. *PLoS medicine* **15**(7), e1002615 (2018)
7. Atlam, E.S., Masud, M., Rokaya, M., Meshref, H., Gad, I., Almars, A.M.: Easdm: Explainable autism spectrum disorder model based on deep learning. *Journal of Disability Research* **3**(1), 20240003 (2024)
8. Chen, S., Zhao, Q.: Attention-based autism spectrum disorder screening with privileged modality. In: *Proceedings of the IEEE/CVF International Conference on Computer Vision*. pp. 1181–1190 (2019)
9. Chong, E., Chanda, K., Ye, Z., Southerland, A., Ruiz, N., Jones, R.M., Rozga, A., Rehg, J.M.: Detecting gaze towards eyes in natural social interactions and its use in child assessment. *Proceedings of the ACM on Interactive, Mobile, Wearable and Ubiquitous Technologies* **1**(3), 1–20 (2017)
10. Christensen, D.L.: Prevalence and characteristics of autism spectrum disorder among children aged 8 years—autism and developmental disabilities monitoring network, 11 sites, united states, 2012. *MMWR. Surveillance summaries* **65** (2016)
11. Crimi, A., Doderio, L., Murino, V., Sona, D.: Case-control discrimination through effective brain connectivity. In: *2017 IEEE 14th International Symposium on Biomedical Imaging (ISBI 2017)*. pp. 970–973. Ieee (2017)
12. Deng, A., Yang, T., Chen, C., Chen, Q., Neely, L., Oyama, S.: Language-assisted deep learning for autistic behaviors recognition. *Smart Health* p. 100444 (2023)
13. Dia, M., Khodabandelou, G., Sabri, A.Q.M., Othmani, A.: Video-based continuous affect recognition of children with autism spectrum disorder using deep learning. *Biomedical Signal Processing and Control* **89**, 105712 (2024)
14. Eslami, T., Saeed, F.: Auto-asd-network: a technique based on deep learning and support vector machines for diagnosing autism spectrum disorder using fmri data. In: *Proceedings of the 10th ACM International Conference on Bioinformatics, Computational Biology and Health Informatics*. pp. 646–651 (2019)
15. Islam, M.F., Manab, M.A., Mondal, J.J., Zabeen, S., Rahman, F.B., Hasan, M.Z., Sadeque, F., Noor, J.: Involution fused convnet for classifying eye-tracking patterns of children with autism spectrum disorder. *arXiv preprint arXiv:2401.03575* (2024)
16. Kollias, K.F., Syriopoulou-Delli, C.K., Sarigiannidis, P., Fragulis, G.F.: The contribution of machine learning and eye-tracking technology in autism spectrum disorder research: A review study. In: *2021 10th International Conference on Modern Circuits and Systems Technologies (MOCASST)*. pp. 1–4. IEEE (2021)
17. Kumar, C.J., Das, P.R.: The diagnosis of asd using multiple machine learning techniques. *International Journal of Developmental Disabilities* pp. 1–11 (2021)
18. Lakkapragada, A., Kline, A., Mutlu, O.C., Paskov, K., Chrisman, B., Stockham, N., Washington, P., Wall, D.P.: The classification of abnormal hand movement to aid in autism detection: Machine learning study. *JMIR Biomedical Engineering* **7**(1), e33771 (2022)
19. Li, H., Parikh, N.A., He, L.: A novel transfer learning approach to enhance deep neural network classification of brain functional connectomes. *Frontiers in neuroscience* p. 491 (2018)
20. Lord, C., Risi, S., DiLavore, P.S., Shulman, C., Thurm, A., Pickles, A.: Autism from 2 to 9 years of age. *Archives of general psychiatry* **63**(6), 694–701 (2006)
21. Marinoiu, E., Zafir, M., Olaru, V., Sminchisescu, C.: 3d human sensing, action and emotion recognition in robot assisted therapy of children with autism. In: *Proceedings of the IEEE conference on computer vision and pattern recognition*. pp. 2158–2167 (2018)
22. Mehmood, F., Ayaz, Y., Ali, S., Amadeu, R.D.C., Sadia, H.: Dominance in visual space of asd children using multi-robot joint attention integrated distributed imitation system. *IEEE Access* **7**, 168815–168827 (2019)
23. Mohan, P., Paramasivam, I.: Feature reduction using svm-rfe technique to detect autism spectrum disorder. *Evolutionary Intelligence* **14**(2), 989–997 (2021)
24. Mujeeb Rahman, K., Monica Subashini, M.: A deep neural network-based model for screening autism spectrum disorder using the quantitative checklist for autism in toddlers (qchat). *Journal of Autism and Developmental Disorders* pp. 1–15 (2021)
25. Negin, F., Ozyer, B., Agahian, S., Kacdioglu, S., Ozyer, G.T.: Vision-assisted recognition of stereotype behaviors for early diagnosis of autism spectrum disorders. *Neurocomputing* **446**, 145–155 (2021)
26. Rajagopalan, S., Dhall, A., Goecke, R.: Self-stimulatory behaviours in the wild for autism diagnosis. In: *Proceedings of the IEEE International Conference on Computer Vision Workshops*. pp. 755–761 (2013)
27. Rajagopalan, S.S., Goecke, R.: Detecting self-stimulatory behaviours for autism diagnosis. In: *2014 IEEE International Conference on Image Processing (ICIP)*. pp. 1470–1474. IEEE (2014)

28. Shrivastava, T., Singh, V., Agrawal, A.: Autism spectrum disorder classification of facial images using xception model and transfer learning with image augmentation. In: International Conference on Neural Information Processing. pp. 170–181. Springer (2022)
29. Tong, Z., Song, Y., Wang, J., Wang, L.: Videomae: Masked autoencoders are data-efficient learners for self-supervised video pre-training. *Advances in neural information processing systems* **35**, 10078–10093 (2022)
30. Volkmar, F.R., Lord, C., Bailey, A., Schultz, R.T., Klin, A.: Autism and pervasive developmental disorders. *Journal of child psychology and psychiatry* **45**(1), 135–170 (2004)
31. Wang, C.Y., Bochkovskiy, A., Liao, H.Y.M.: YOLOv7: Trainable bag-of-freebies sets new state-of-the-art for real-time object detectors. In: Proceedings of the IEEE/CVF conference on computer vision and pattern recognition. pp. 7464–7475 (2023)
32. Wang, Z., Xu, K., Liu, H.: Screening early children with autism spectrum disorder via expressing needs with index finger pointing. In: Proceedings of the 13th International Conference on Distributed Smart Cameras. pp. 1–6 (2019)
33. Washington, P., Kline, A., Mutlu, O.C., Leblanc, E., Hou, C., Stockham, N., Paskov, K., Chrisman, B., Wall, D.: Activity recognition with moving cameras and few training examples: applications for detection of autism-related headbanging. In: Extended abstracts of the 2021 CHI conference on human factors in computing systems. pp. 1–7 (2021)
34. Wei, P., Ahmedt-Aristizabal, D., Gammulle, H., Denman, S., Armin, M.A.: Vision-based activity recognition in children with autism-related behaviors. *Heliyon* (2023)
35. Zheng, W., Eilam-Stock, T., Wu, T., Spagna, A., Chen, C., Hu, B., Fan, J.: Multi-feature based network revealing the structural abnormalities in autism spectrum disorder. *IEEE Transactions on Affective Computing* **12**(3), 732–742 (2019)